

**ATHENA – FIRST PRODUCTION OF COLD  
ANTIHYDROGEN AND BEYOND**

A. KELLERBAUER<sup>1</sup>, M. AMORETTI<sup>2,3</sup>, C. AMSLER<sup>4</sup>, G. BONOMI<sup>1</sup>,  
P. D. BOWE<sup>5</sup>, C. CANALI<sup>2,3</sup>, C. CARRARO<sup>2,3</sup>, C. L. CESAR<sup>6</sup>,  
M. CHARLTON<sup>5</sup>, M. DOSER<sup>1</sup>, A. FONTANA<sup>7,8</sup>, M. C. FUJIWARA<sup>9</sup>,  
R. FUNAKOSHI<sup>10</sup>, P. GENOVA<sup>7,8</sup>, J. S. HANGST<sup>11</sup>, R. S. HAYANO<sup>10</sup>,  
I. JOHNSON<sup>4</sup>, L. V. JØRGENSEN<sup>5</sup>, V. LAGOMARSINO<sup>2,3</sup>, R. LANDUA<sup>1</sup>,  
E. LODI RIZZINI<sup>12,8</sup>, M. MACRÌ<sup>2,3</sup>, N. MADSEN<sup>11</sup>, G. MANUZIO<sup>2,3</sup>,  
D. MITCHARD<sup>5</sup>, P. MONTAGNA<sup>7,8</sup>, H. PRUYS<sup>4</sup>, C. REGENFUS<sup>4</sup>,  
A. ROTONDI<sup>7,8</sup>, G. TESTERA<sup>2,3</sup>, A. VARIOLA<sup>5</sup>, L. VENTURELLI<sup>12,8</sup>,  
D. P. VAN DER WERF<sup>5</sup>, Y. YAMAZAKI<sup>9</sup>, AND N. ZURLO<sup>12,8</sup>

<sup>1</sup>*Department of Physics, CERN, 1211 Genève 23, Switzerland*

<sup>2</sup>*Dipartimento di Fisica, Università di Genova, 16146 Genova, Italy*

<sup>3</sup>*INFN Sezione di Genova, 16146 Genova, Italy*

<sup>4</sup>*Physik-Institut, University of Zurich, 8057 Zürich, Switzerland*

<sup>5</sup>*Department of Physics, University of Wales Swansea, Swansea SA2 8PP, UK*

<sup>6</sup>*Instituto de Física, Universidade Federal do Rio de Janeiro, Rio de Janeiro  
21945-970, Brazil*

<sup>7</sup>*Dipartimento di Fisica Nucleare e Teorica, Università di Pavia, 27100 Pavia,  
Italy*

<sup>8</sup>*INFN Sezione di Pavia, 27100 Pavia, Italy*

<sup>9</sup>*Atomic Physics Laboratory, RIKEN, Saitama 351-0198, Japan*

<sup>10</sup>*Department of Physics, University of Tokyo, Tokyo 113-0033, Japan*

<sup>11</sup>*Department of Physics and Astronomy, University of Aarhus, 8000 Aarhus C,  
Denmark*

<sup>12</sup>*Dipartimento di Chimica e Fisica per l'Ingegneria e per i Materiali,  
Università di Brescia, 25123 Brescia, Italy*

(ATHENA Collaboration)

Atomic systems of antiparticles are the laboratories of choice for tests of CPT symmetry with antimatter. The ATHENA experiment was the first to report the production of copious amounts of cold antihydrogen in 2002. This article reviews some of the insights that have since been gained concerning the antihydrogen production process as well as the external and internal properties of the produced anti-atoms. Furthermore, the implications of those results on future prospects of symmetry tests with antimatter are discussed.

## 1. Introduction

According to the CPT theorem<sup>1</sup>, all physical laws are invariant under the combined operations of charge conjugation, parity (reversal of the spatial configuration), and time reversal. Since CPT transforms an elementary particle into its antiparticle, their fundamental properties such as mass, charge, and magnetic moment, are either exactly equal or exactly opposed. This predestines antimatter for tests of CPT symmetry. Due to the fact that atomic spectroscopy on the transition between the ground and first excited states (1s–2s) of hydrogen has been carried out to  $10^{-14}$  relative precision<sup>2</sup>, this transition is also being targeted for CPT tests with hydrogen and antihydrogen ( $\bar{\text{H}}$ ). In addition to atomic spectroscopy, antimatter gravity tests are being considered. These could be carried out by gravity interferometry<sup>3</sup> or in atomic fountains, in analogy with current studies on ordinary matter in such setups<sup>4</sup>.

Two dedicated experiments, ATHENA<sup>5</sup> and ATRAP<sup>6</sup>, have been set up at CERN’s Antiproton Decelerator (AD)<sup>7</sup> since 1998 with the goal of producing sufficient amounts of antihydrogen to ultimately allow precision atomic spectroscopy and a comparison of its atomic spectrum with that of hydrogen. A production of large amounts of  $\bar{\text{H}}$  was first demonstrated by ATHENA<sup>8</sup> and later by ATRAP<sup>9</sup>, using very similar schemes for antihydrogen production but different detection techniques. In the time since these independent proofs of principle, the main challenges have been to investigate the parameters that govern efficient  $\bar{\text{H}}$  production and the internal and external properties of the produced antihydrogen.

## 2. Setup and principle

The ATHENA apparatus<sup>5</sup> consists of three main components, shown in Fig. 1: The antiproton ( $\bar{p}$ ) capture trap, the mixing trap, and the positron ( $e^+$ ) source and accumulator. The former two are located in the 3-T field of a superconducting magnet whose bore is kept at liquid-nitrogen temperature. A liquid-helium cryostat, whose cold nose protrudes into the magnet bore and encloses the trap, reduces the temperature of the trap region further to about 15 K.

The bunch of about  $2\text{--}3 \times 10^7$  antiprotons that is extracted from the AD after every deceleration and cooling cycle undergoes a final deceleration step in a thin ( $\approx 50 \mu\text{m}$ ) degrader foil. The foil’s thickness is chosen in order to optimize the fraction of  $\bar{p}$  that can be trapped by the capture trap’s high-voltage electrodes (5 kV potential). In the capture trap, the

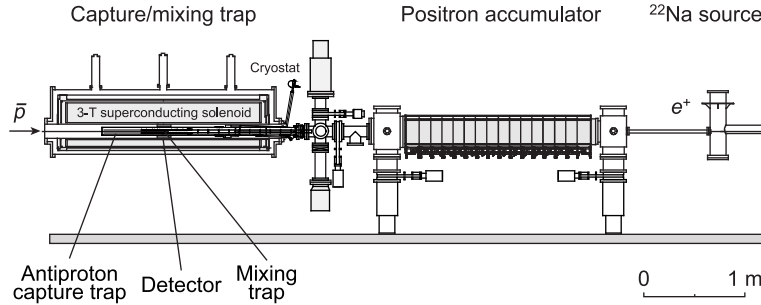


Figure 1. Overview of the ATHENA apparatus. Shown on the left is the superconducting 3-T solenoid magnet which houses the capture trap, the mixing trap, and the antihydrogen annihilation detector. On the right, the radioactive sodium source for the positron production and the 0.14-T positron accumulation Penning trap.

confined antiprotons cool in Coulomb collisions with an electron plasma that was loaded prior to the  $\bar{p}$  capture and allowed to cool by emission of synchrotron radiation. Typically, two  $\bar{p}$  spills from the AD are stacked in the capture trap, resulting in about  $10^4$   $\bar{p}$  ready for mixing. Simultaneously, positrons produced in the  $\beta$  decay of the radionuclide  $^{22}\text{Na}$  are moderated, then cooled in collisions with nitrogen buffer gas and accumulated in a low-field Penning trap at room temperature.

After the independent  $\bar{p}$  stacking and  $e^+$  accumulation phases, the axial potential in the mixing trap is brought into a so-called nested configuration<sup>10</sup>. Figure 2(a) shows how this potential shape allows both positively and negatively charged particles to be simultaneously confined. The central well of this nested trap is then first filled with the  $\approx 5 \times 10^7$  accumulated positrons. Just like the electrons in the capture trap, these cool to the ambient temperature of about 15 K by emitting synchrotron radiation. The antiprotons are transferred into a small lateral well and then launched into the mixing region with a relative energy of 30 eV. They oscillate between the lateral confines of the nested well, repeatedly traverse the  $e^+$  plasma, and rapidly cool in Coulomb collisions with the positrons. After some tens of ms, antihydrogen production spontaneously sets in with initial rates of several 100 Hz.

The neutral  $\bar{\text{H}}$  atoms thus produced in the center of the mixing trap are no longer affected, to first order, by the electrical and magnetic fields used for the charged-particle confinement. They leave the interaction region with a momentum that is essentially equal to that of the  $\bar{p}$  just before  $\bar{\text{H}}$  formation. When these anti-atoms impinge upon the Penning trap electrodes,

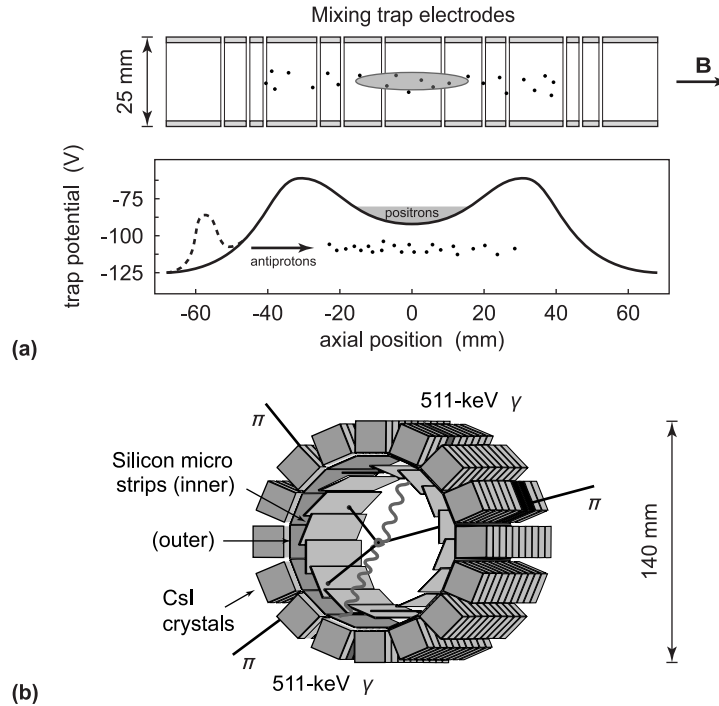


Figure 2. (a) Detailed sketch of the mixing trap, which is operated in a nested-trap configuration. The graph shows the axial trap potential before (dashed line) and after (solid line) the antiproton injection. (b) Sketch of the antihydrogen annihilation detector. With its highly granular silicon strip and CsI crystal modules, it allows a direct and unambiguous detection of  $\bar{\text{H}}$  production.

their constituents immediately annihilate with ordinary matter. The signal of these destructive events is recorded with the antihydrogen annihilation detector that surrounds the mixing trap. A sketch of this detector is shown in Fig. 2(b). It consists of 8192 silicon strips in two layers for the detection of the charged pions created in the  $\bar{p}$  annihilation with a proton or a neutron and 192 cesium iodide crystals that record the (mainly back-to-back)  $\gamma$  rays from the  $e^+e^-$  annihilation. Despite its extremely compact dimensions, it allows a three-dimensional reconstruction of the charged-particle vertex with a resolution of 4 mm and a spatial and temporal correlation of the  $\bar{p}$  and  $e^+$  signals for an unambiguous identification of  $\bar{\text{H}}$  formation.

As an example for event reconstruction, Fig. 3 illustrates the signal of the first production of cold antihydrogen<sup>8</sup> in 2002. In Fig. 3(a), the az-

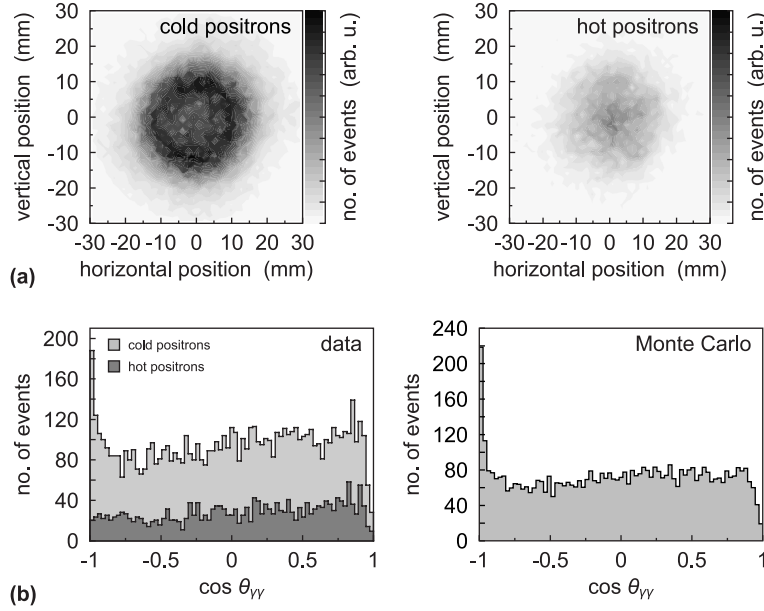


Figure 3. Signal of the first production of cold antihydrogen with ATHENA<sup>8</sup>. (a) Charged-pion vertex distribution as a function of the azimuthal coordinates. (b) Opening-angle distribution of the photons recorded in coincidence with the charged-particle hits, as seen from the charged-particle vertex.

imuthal distribution of reconstructed vertices from the  $\bar{p}$  annihilation is shown. In the left panel, where the positrons are in thermal equilibrium with the trap at 15 K (“cold mixing”), the largest numbers of events are recorded in a ring located at the position of the electrodes (25 mm diameter). When the positron plasma is heated by means of a radiofrequency (RF) excitation of the axial plasma modes<sup>11</sup> (“hot mixing”),  $\bar{\text{H}}$  production is suppressed and a smaller number of events, due to  $\bar{p}$  annihilations with residual gas, is recorded in the center of the trap (right panel). Figure 3(b) shows the distribution of the opening angle of the two 511-keV  $\gamma$  rays recorded in time coincidence with the charged-particle hits, as seen from the charged-particle vertex. In the left panel, a clear excess at an opening angle of  $180^\circ$  is present for cold positrons, while it is suppressed when the positron plasma is heated. The right panel shows the good agreement of the data with Monte-Carlo simulations. The 131(22) fully reconstructed events that constitute the peak in the left panel of Fig. 3(b) correspond to a total number of about 50 000 produced  $\bar{\text{H}}$  atoms for this partial dataset

of 2002. A complete analysis of the 2002 data, together with more detailed Monte Carlo simulations, showed that the instantaneous trigger rate from the silicon detector is a good proxy for antihydrogen production, with 65% of all triggers over the entire mixing cycle due to annihilating antihydrogen atoms<sup>12</sup>.

### 3. Recent results

For precise antimatter studies, it is not sufficient to merely produce large numbers of antihydrogen. A fair knowledge of the temperature and kinetic-energy distributions of the produced  $\bar{\text{H}}$  is required in order to estimate the fraction of anti-atoms which can be trapped. The  $\bar{\text{H}}$  atoms must also be produced in a well-defined internal quantum state, if possible the ground state. In this section, some results on the latter question, based on an investigation of the  $\bar{\text{H}}$  formation process, are presented.

#### 3.1. *Antihydrogen production 2002/2003*

As a prerequisite for any quantitative studies on antihydrogen formation, the offline data analysis must allow a precise determination of the number of produced  $\bar{\text{H}}$  anti-atoms. In order to achieve this, one or several observables, such as the radial vertex distribution or the  $2\gamma$  opening angle distribution, can be considered as a linear combination of a pure  $\bar{\text{H}}$  signal (Monte-Carlo simulation of annihilations on the trap electrodes) and background. Since the background is expected to be mainly due to  $\bar{p}$  annihilations with residual gas, it can be represented by the signal obtained from runs in which the  $e^+$  were heated to several 1000 K, thereby inhibiting  $\bar{\text{H}}$  production. The total antihydrogen production of 2002 and 2003 obtained in this way is summarized in Tab. 1. It shows that ATHENA has produced more than  $10^6$   $\bar{\text{H}}$  anti-atoms since its start of operations and that the production efficiency in terms of captured antiprotons from the AD is between 10 and 20%.

#### 3.2. *Recombination process*

The formation of antihydrogen by direct capture of a positron onto an atomic orbit around an antiproton does not simultaneously conserve energy and momentum. The involvement of a third particle is needed in order to respect these conservation laws. That particle can either be a photon in the case of (spontaneous) radiative recombination (SRR)<sup>13</sup> or a second positron in three-body recombination (TBR)<sup>14</sup>. These two processes are

Table 1. Comparative summary of ATHENA's antihydrogen production in 2002 and 2003.

	Cold mixing 2002	Cold mixing 2003
Total no. of cycles	341	416
Cycle duration	180 s	70 s
Total mixing time	17.1 h	8.1 h
Injected $\bar{p}$	$2.92 \times 10^6$	$5.07 \times 10^6$
Produced $\bar{\text{H}}$	$4.94 \times 10^5$	$7.04 \times 10^5$
Production efficiency	16.9%	13.9%
Avg. $\bar{\text{H}}$ production rate	8.0(4) Hz	24.2(1.3) Hz
$\bar{\text{H}}$ fraction of signal	65(5)%	74(3)%

predicted to have vastly different cross-sections and recombination rates, with TBR expected to be the dominant process at ATHENA's experimental conditions. The most important difference with a view to precision studies lies in the fact that SRR populates low-lying states ( $n < 10$ ) and TBR highly excited Rydberg states ( $n \gg 10$ ). The two mechanisms also exhibit different dependencies on the positron temperature (SRR:  $\propto T^{-0.63}$ ; TBR:  $\propto T^{-4.5}$ ) and density (SRR:  $\propto n_{e^+}$ ; TBR:  $\propto n_{e^+}^2$ ), which can allow to distinguish between them.

In order to determine the temperature dependence of  $\bar{\text{H}}$  production, we have performed mixing cycles with RF heating at various amplitudes applied to the positron plasma<sup>15</sup>. The positron temperature increase was measured with ATHENA's plasma diagnostics system<sup>11</sup> by resonant excitation and detection of the axial plasma modes. In Fig. 4, the background-corrected integrated number of triggers (left) and peak trigger rate (right) as possible proxies for  $\bar{\text{H}}$  production are shown as a function of the positron temperature, assuming an equilibrium temperature of 15 K. Neither of these plots shows the characteristics of a simple power law (a straight line in these logarithmic plots), but a best fit to the data yields a behavior of the form  $\propto T^{-0.7(2)}$ , close to that expected from radiative recombination. However, the observed event rates are between 1 and 2 orders of magnitude higher than expected for this recombination process.

The second access to the recombination process is via the positron density dependence. For this purpose, we have analyzed the 2003 data with a view to varying positron plasma density<sup>16</sup>. Standard cold mixing runs with positron plasma densities between  $3 \times 10^8/\text{cm}^3$  and  $1.5 \times 10^9/\text{cm}^3$

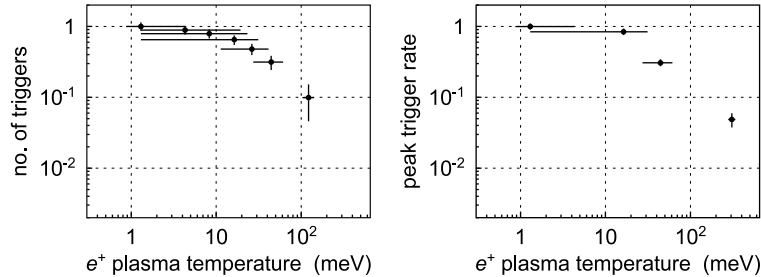


Figure 4. Dependence of the background-corrected integrated total number of charged-particle triggers per mixing cycle (left) and the peak trigger rate (left) on the positron plasma temperature<sup>15</sup>. The number of triggers and trigger rate have been normalized to the signal for an  $e^+$  temperature of 1 meV. Note the logarithmic scale.

have been identified. However, this analysis is complicated by the fact that under ATHENA’s typical experimental conditions, the  $\bar{p}$  cloud has a much larger radial extent than the  $e^+$  plasma. This means that the number of interacting antiprotons strongly depends on their radial density distribution. Measurements of this distribution are therefore required to extract the positron density dependence of  $\bar{H}$  production.

#### 4. Antihydrogen spectroscopy within the framework of the Standard-Model Extension

Any measured difference in the hydrogen and antihydrogen atomic spectra would be a clear and unambiguous signal for CPT violation. On the other hand, a theoretical framework for such symmetry breaking can indicate which transitions are particularly suited for an experimental search. The Standard Model Extension<sup>17</sup> incorporates spontaneous CPT and Lorentz breaking at a fundamental level. It is an extension of the Standard Model that preserves energy and momentum conservation, gauge invariance, renormalizability, and micro-causality.

Within this framework, the sensitivity to CPT- and Lorentz-violating terms of spectroscopic experiments on H and  $\bar{H}$  confined in a magnetic trap can be predicted. Consider the energy states of (anti)hydrogen with zero angular momentum ( $l = 0$ ), confined in a magnetic trap with axial solenoidal field and radial multipole magnetic fields. These states are subject to hyperfine as well as Zeeman splitting, as shown in Fig. 5. Before the excitation, only the low-field-seeking states  $|c\rangle_1$  and  $|d\rangle_1$  are confined in a magnetic trap. It has been shown<sup>18</sup> that the CPT-violating term  $b_3^s$  shifts



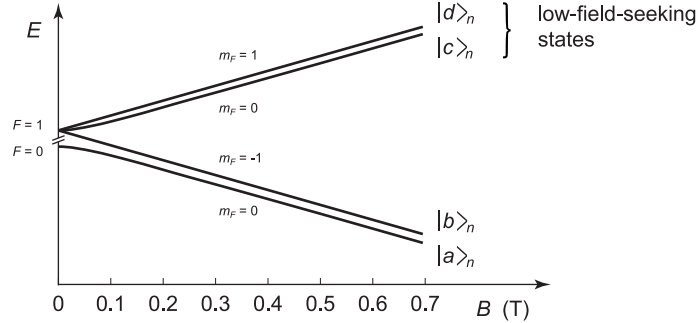


Figure 5. Hyperfine and Zeeman splitting of (anti)hydrogen confined in a magnetic field for states with zero angular momentum.

all  $|d\rangle_n$  states by the same amount, both in  $\text{H}$  and in  $\overline{\text{H}}$ , and the CPT-violating effect is thus suppressed by a factor  $\alpha^2/8\pi$  in the  $|d\rangle_1 \rightarrow |d\rangle_2$  transition. The transition  $|c\rangle_1 \rightarrow |c\rangle_2$  between the mixed-spin states does potentially produce an unsuppressed frequency shift due to the  $n$  dependence of the hyperfine splitting. This shift is different in  $\text{H}$  and in  $\overline{\text{H}}$  and leads both to diurnal variations in the frequency difference and to a non-zero instantaneous difference. However, this transition is field-dependent and thus subject to Zeeman broadening in inhomogeneous magnetic fields.

As an alternative, it was therefore suggested<sup>18</sup> to consider a transition between hyperfine levels of the ground state ( $n = 1$ ) at the field-independent transition point  $B \approx 0.65$  T. The transition  $|d\rangle_1 \rightarrow |c\rangle_1$  in  $\text{H}$  and in  $\overline{\text{H}}$  is then subject to potential diurnal variations, and the instantaneous difference  $\Delta\nu_{cd}$  between these transitions in hydrogen and antihydrogen is directly proportional to the CPT-violating term  $b_3^p$ . Based on these considerations, future antihydrogen spectroscopy experiments will include comparisons of the hydrogen and antihydrogen hyperfine structure<sup>19</sup>.

## 5. Conclusions and outlook

With the first production of copious amounts of cold antihydrogen, many of the challenges on the way to high-precision CPT tests with antimatter have been surmounted, but many more still remain. Future high-precision spectroscopic and interferometric measurements on antimatter atoms are contingent upon the ability to confine neutral  $\overline{\text{H}}$  atoms and to cool them with Lyman- $\alpha$  lasers. Our results on the temperature dependence of  $\overline{\text{H}}$  production suggest on the one hand that an appreciable fraction of the

antihydrogen may be produced in low-lying states accessible to precision atomic spectroscopy. On the other hand, recombination possibly sets in before complete thermalization of the antiprotons, thereby reducing the fraction of produced antihydrogen that can be confined in a magnetic trap. Further studies on antihydrogen production in a nested Penning trap are required to clarify these points. In parallel, tests with ordinary matter on the simultaneous confinement of charged and neutral particles in electromagnetic traps are being carried out in order to establish parameters for the efficient preparation of trapped antihydrogen for symmetry tests.

### Acknowledgments

This work was supported by the funding agencies INFN (Italy), CNPq (Brazil), MEXT (Japan), SNF (Switzerland), SNF (Denmark), and EPSRC (United Kingdom).

### References

1. W. Pauli, *Il Nuovo Cimento* **6** (1957) 6.
2. M. Niering *et al.*, *Phys. Rev. Lett.* **84** (2000) 5496.
3. T. J. Philips, *Hyp. Int.* **109** (1997) 357.
4. A. Peters *et al.*, *Nature* **400** (1999) 849.
5. M. Amoretti *et al.*, *Nucl. Instrum. Methods A* **518** (2004) 679.
6. G. Gabrielse *et al.*, *Phys. Lett. B* **455** (1999) 311.
7. J. Y. Hémerly and S. Maury, *Nucl. Phys. A* **655** (1999) 345c.
8. M. Amoretti *et al.*, *Nature* **419** (2002) 456.
9. G. Gabrielse *et al.*, *Phys. Rev. Lett.* **89** (2002) 213401.
10. G. Gabrielse *et al.*, *Phys. Lett. A* **129** (1988) 38.
11. M. Amoretti *et al.*, *Phys. Rev. Lett.* **91** (2003) 055001.
12. M. Amoretti *et al.*, *Phys. Lett. B* **578** (2004) 23.
13. J. Stevefelt *et al.*, *Phys. Rev. A* **12** (1975) 1246.
14. M. E. Glinsky *et al.*, *Phys. Fluids B* **3** (1991) 1279.
15. M. Amoretti *et al.*, *Phys. Lett. B* **583** (2004) 59.
16. G. Bonomi *et al.*, to be published.
17. D. Colladay and V. A. Kostelecký, *Phys. Rev. D* **55** (1997) 6760.
18. R. Bluhm, V. A. Kostelecký, and N. Russell, *Phys. Rev. Lett.* **82** (1999) 2254.
19. R. Hayano *et al.*, these proceedings.